Journal for ImmunoTherapy of Cancer

Targeting mesothelin-CD24 axis repolarizes tumor-associated macrophages to potentiate PD-1 blockade therapy in high-grade serous ovarian cancer

Yujing Zhong,[1] Yiying Wang,[1,2] Chenyang Wang,[1] Kankan Cao,[1] Xueling Wang,[1] Xuyao Xu,[1] Moran Yang,[1,2] Guodong Zhang,[1,2] Haiou Liu ,[1,2] Jiaqi Lu[1,2]

To cite: Zhong Y, Wang Y, Wang C, *et al*. Targeting mesothelin-CD24 axis repolarizes tumor-associated macrophages to potentiate PD-1 blockade therapy in high-grade serous ovarian cancer. *Journal for ImmunoTherapy of Cancer* 2025;**13**:e011230. doi:10.1136/jitc-2024-011230

► Additional supplemental material is published online only. To view, please visit the journal online (https://doi.org/10.1136/jitc-2024-011230).

Accepted 03 February 2025

[1]Shanghai Key Laboratory of Female Reproductive Endocrine Related Diseases, Obstetrics and Gynecology Hospital of Fudan University, Shanghai, China
[2]Department of Gynecology, Obstetrics and Gynecology Hospital, Obstetrics and Gynecology Hospital of Fudan University, Shanghai, China

Correspondence to
Dr Jiaqi Lu;
lujiaqidoc@hotmail.com

Dr Haiou Liu;
liuhaiou@fudan.edu.cn

ABSTRACT

Background High-grade serous ovarian cancer (HGSOC) is a highly aggressive malignancy marked by an immunosuppressive tumor microenvironment that hinders effective immune responses. A key feature of this environment is the extensive infiltration of myeloid cells, which contributes to immune evasion. This study explored how mesothelin (MSLN), a tumor-associated antigen, modulates the expression of CD24, an emerging target for immune modulation, and its role in promoting immune evasion in HGSOC. Understanding these underlying mechanisms is crucial for enhancing the efficacy of immune checkpoint blockade (ICB) therapies and improving outcomes in patients with HGSOC.

Methods We analyzed the expression of MSLN in HGSOC samples and examined its correlation with clinical outcome. In vitro and in vivo models were used to explore how MSLN influences CD24 expression and the polarization of tumor-associated macrophages (TAMs). We also investigated the role of MSLN in the activation of Wnt/β-catenin signaling and its impact on T-cell function and antitumor immunity. The effects of *Msln* knockdown on CD24 expression and the response to anti-programmed cell death protein-1 (PD-1) therapy were evaluated in syngeneic mouse models.

Results MSLN expression was found to be significantly elevated in HGSOC, with high MSLN levels correlating with poor prognosis and resistance to ICB. MSLN upregulated CD24 and promoted the protumorigenic polarization of TAMs, contributing to T-cell dysfunction. Mechanistically, MSLN activated Wnt/β-catenin signaling, which in turn enhanced CD24 expression. This activation forms a positive feedback loop that further promotes MSLN transcription. In contrast, *Msln* knockdown reduced CD24 expression, relieved cytotoxic T-cell suppression, and significantly improved the efficacy of anti-PD-1 therapy in syngeneic models.

Conclusions This study elucidates the critical role of MSLN in immune evasion in HGSOC and its underlying mechanisms. Targeting MSLN in combination with ICB is a promising strategy to enhance the efficacy of immunotherapy and improve patient outcomes in HGSOC.

WHAT IS ALREADY KNOWN ON THIS TOPIC

⇒ In high-grade serous ovarian cancer (HGSOC), the tumor microenvironment (TME) is often immunosuppressive, primarily due to the infiltration of myeloid-derived cells that hinder immune function. Although immune checkpoint blockades (ICBs) have shown efficacy in other cancers, their success in HGSOC remains limited. Mesothelin (MSLN) is a glycoprotein that is overexpressed in multiple cancers, including HGSOC, and is associated with poor prognosis and resistance to immunotherapy.

WHAT THIS STUDY ADDS

⇒ This study provides novel insights into how MSLN contributes to immune evasion in HGSOC by modulating CD24 expression through activation of the Wnt/β-catenin signaling pathway. The results showed that MSLN promoted protumorigenic polarization of tumor-associated macrophages and induced T-cell dysfunction. Importantly, this study identified a positive feedback loop that enhances MSLN transcription, further promoting immunosuppression. Moreover, MSLN knockdown led to reduced CD24 expression, alleviated cytotoxic T-cell suppression, and improved the efficacy of anti-programmed cell death protein-1 therapy in preclinical models, offering potential strategies for enhancing immunotherapy.

HOW THIS STUDY MIGHT AFFECT RESEARCH, PRACTICE OR POLICY

⇒ This study underscores the critical role of MSLN in immune evasion within the TME of HGSOC, thus, positioning MSLN as a promising therapeutic target. By targeting MSLN in combination with ICB, this approach could offer a more effective immunotherapy strategy for improving the clinical outcomes in patients with HGSOC. These findings could drive the development of novel combination therapies and pave the way for clinical trials aimed at improving the prognosis of patients with HGSOC.

INTRODUCTION

Although most immune checkpoint blockades (ICBs) exhibit limited efficacy,[1] mesothelin (MSLN) has emerged as a key immunosuppressive mediator.[2 3] MSLN, a membrane glycoprotein overexpressed in mesothelioma, non-small cell lung cancer, pancreatic cancer, and ovarian cancer, is minimally expressed in a few selected normal tissues,[4 5] making it an attractive target for immunotherapy. For example, the use of chimeric antigen receptor NK-92 cells to target MSLN in ovarian cancer.[6] Complementing these findings, Jiang *et al* observed that combining the MSLN-targeted immunotoxin LMB-100 with anti-programmed cell death protein-1 (PD-1) antibody significantly improved outcomes in patients with mesothelioma, underscoring the synergy between immune checkpoint inhibitors and targeted therapies.[7] Additionally, in mouse tumors, LMB-100 treatment induces the formation of tertiary lymphoid structures (TLS) by upregulating-related genes and activating antitumor immunity.[8] Despite these advances, challenges remain in identifying reliable biomarkers for therapeutic response. For instance, Katz *et al* found that while serum soluble MSLN-related protein and fibulin-3 correlated with tumor volumes in mesothelioma, they lacked predictive value in immunotherapy trials.[9] Despite the progress in mesothelioma,[5 10] pancreatic[11–13] and lung cancers,[14] the role of MSLN-targeted therapies in high-grade serous ovarian cancer (HGSOC) and its impact on tumor microenvironment (TME) remodeling remains underexplored.

The TME is dynamically shaped by the dysregulation of key signaling pathways, such as the Wnt/β-catenin pathway—a complex network of protein interactions closely linked to cancer progression.[15 16] This pathway is pivotal in sustaining cancer stem cell renewal, driving uncontrolled cell proliferation and differentiation, ultimately contributing to TME remodeling and impacting treatment response.[17] Mutational biases vary across cancer types, with APC (Adenomatous Polyposis Coli) mutations being particularly prevalent in ovarian cancer, underscoring the significance of Wnt-driven alterations in tumor development.[18] In view of these challenges, elucidating the mechanisms by which Wnt-mediated reshape the TME is crucial for screening patients for ICB therapy and enhanced efficacy of ICB therapy.

In this study, we present findings from HGSOC organoids and murine ovarian cancer models, demonstrating that MSLN upregulates CD24 expression via the activation of the Wnt/β-catenin pathway. Targeting MSLN significantly enhanced the efficacy of anti-PD-1 treatment in HGSOC organoids and murine models by remodeling the TME, promoting a favorable tumor-associated macrophages (TAMs) phenotype, activating $CD8^+$ T cells, and further increasing the abundance of T-cell exhaustion progenitor cells (Tpex).

MATERIALS AND METHODS

Patient sample collection

The Discovery cohort (n=120) was obtained from the Gynecology and Obstetrics Hospital of the Fudan University between March 2013 and November 2015. The Validation cohort (n=160) was obtained from Shanghai Cancer Center between January 2012 and October 2019. All enrolled participants (n=280) who underwent surgery completed follow-up, with no attrition observed (attrition rate=0%). This observational study did not involve randomization, and participants were consecutively recruited post-surgery and followed-up prospectively. Fresh tumor tissues from 76 patients with HGSOC were obtained from our hospital and subjected to flow cytometry analysis (n=48) and ex vivo intervention (n=28). All HGSOC specimens were surgically resected from the primary site and were histologically verified. Detailed clinicopathological characteristics of the patients are shown in online supplemental table 1. The pathological staging and histological classification were based on the FIGO (International Federation of Gynecology and Obstetrics) criteria (2018). The overall survival (OS) was calculated from the date of surgery to the last follow-up or death. Follow-up for the Discovery cohort continued until March 2019, while the Validation cohort was monitored until September 2023. None of the patients with HGSOC received any therapeutic intervention before surgery.

Construction of stably transfected cell line

ID8agg-luc cells and OV2944-HM1-luc cells were transduced with *Msln*-targeting short hairpin RNA (shRNA) lentivirus at a multiplicity of infection of 20. Stable cell lines were subsequently established by selection with hygromycin B (#10687010, Invitrogen, RRID: SCR_025910). The knockdown efficiency of each shRNA sequence was first measured by real-time PCR and flow cytometry, and only shRNAs showing at least 60% knockdown were chosen for further experiments. Full-length *Cd24a* was cloned into a pcDNA3.1 (+) vector. The plasmid was sequenced prior to transfection to confirm the correct nucleotide sequence. pcDNA3.1-*Cd24a* was transfected into ID8agg-luc cells using Lipofectamine 3000 reagent (#L300001, Invitrogen, RRID: SCR_025911), according to the manufacturer's recommendations, and selected with puromycin to establish a stable cell line. The target sequences are listed in online supplemental table 2.

Flow cytometry

Fresh tissues from mouse and human tumors were collected, digested with a gentleMACS Dissociator (#130-093-235, Bio X Cell, RRID: SCR_025922), and passed through a Falcon 100 µm cell strainer (#352360, CORNING, RRID: SCR_025923). After washing with ice-cold phosphate-buffered saline and lysing for red blood cell removal with 1×RBC Lysis Buffer (#2881585, eBioscience, RRID: SCR_025960), the purified single-cell suspensions were blocked with Fc receptor blocking reagent (#156604, BioLegend, RRID: SCR_025924) to

prevent non-specific binding. Fluorescence-conjugated antibodies (online supplemental table 3) targeting cell surface markers were added and the cells were incubated in the dark at 4°C for 30 min. Before intracellular and intranuclear staining, samples were treated with FOXP3/Transcription Factor Staining Buffer Set. To control background staining, parallel cells were stained with isotype-matched antibodies. Viable cells were identified using the Zombie Aqua Fixable Viability Kit (#423102, BioLegend, RRID: SCR_025925). Fluorescence data were collected on a CytoFLEX flow cytometer (RRID: SCR_025926, Beckman Coulter) and analyzed using FlowJo software V.10.8.1 (RRID: SCR_008520, Tree Star). The gating strategies for flow cytometry analyses of HGSOC specimens and mouse samples are detailed in online supplemental figures 1,2.

RNA extraction and quantitative reverse transcription PCR

Total RNA was extracted using the FastPureRNA Isolation Kit V2 (#RC112-01, Vazyme, RRID: SCR_02592). Total RNA was reverse-transcribed using the HiScript III RT SuperMix Kit (#R323-01, Vazyme, RRID: SCR_025929). Quantitative (qPCR) was performed using the Taq Pro Universal SYBR qPCR Master Mix kit (#Q712-02, Vazyme, RRID: SCR_025930) on an ABI QuantStudio 3 Flex instrument (Thermo Fisher Scientific, RRID: SCR_025959). Gene expression was normalized to that of GAPDH in each sample, using the comparative threshold cycle method. Primers used in this study are listed in online supplemental table 4.

Western blotting

Tumor cells were lysed in radioimmunoprecipitation assay buffer (#89900, Thermo Fisher Scientific, RRID: SCR_025931) with protease and phosphatase inhibitors (#87786, Thermo Fisher Scientific, RRID: SCR_025932). Protein quantification was performed using the Pierce Bicinchoninic Acid Protein Assay Kit (#A55860, Thermo Fisher Scientific, RRID: SCR_025933). The protein samples were loaded onto 10% sodium dodecyl sulfate-polyacrylamide gel electrophoresis gels. After electrophoresis, proteins were transferred onto polyvinylidene difluoride (PVDF) membranes. After blocking, PVDF membranes were incubated with primary antibodies (online supplemental table 5) at 4°C overnight. After 1 hour of incubation with secondary antibodies at room temperature, protein bands were detected using an enhanced Chemiluminescence Detection Kit (#PA112, TIANGEN Biotech, RRID: SCR_025935) and an Alliance MINI HD 6 Analyzer (UVITEC, RRID: SCR_025936).

Differentially expressed genes and pathway enrichment analysis

The R package "DESeq2" (V.1.42.1, RRID: SCR_015687) was used to identify differentially expressed genes (DEGs) between the two groups. Significantly enriched pathways were obtained through Gene Set Enrichment Analysis (GSEA, RRID: SCR_003199) using the Gene Ontology (RRID: SCR_002811), Kyoto Encyclopedia of Genes and Genomes (RRID: SCR_012773) and WikiPathways (RRID: SCR_002134) databases with the R package "clusterProfiler" (V.4.12.0, RRID: SCR_016884). GSEA gene sets are provided in online supplemental table 6.

Statistical analysis

Statistical analyses were performed using GraphPad Prism V.9.2.0 (RRID: SCR_002798) or MedCalc V.19.0.5 (RRID: SCR_015044). The D'Agostino and Pearson omnibus normality test was applied to assess the normality of the data in each comparison. For data sets that followed a Gaussian distribution, parametric tests were performed, including the two-tailed unpaired Student's t-test, one-way or two-way analysis of variance (ANOVA) with Tukey's post hoc test for multiple comparisons. In cases where the data did not follow a Gaussian distribution, non-parametric tests were applied, such as Mann-Whitney U test, one-way ANOVA with Kruskal-Wallis and Dunn's post hoc test for multiple comparisons, or Spearman's correlation. The χ^2 test was used to compare categorical variables between independent groups. The prognostic significance of the risk factors was assessed using Cox proportional hazards regression models for both univariate and multivariate analyses. Survival curves were generated using the Kaplan-Meier method, and survival times between subgroups were compared using the log-rank test. All experiments were performed with at least two independent replicates. Data are presented as mean±SD, and a two-tailed p value<0.05 was considered statistically significant.

RESULTS

Enhanced MSLN expression is associated with poor prognosis in HGSOC and may contribute to resistance against ICB therapy

We first analyzed the relationship between MSLN expression and survival outcomes in three independent cohorts (online supplemental figure 3A–C). In all cohorts, higher MSLN expression was significantly associated with reduced OS. Further analysis demonstrated a link between elevated MSLN expression and advanced FIGO stage in both the Discovery and Validation cohorts (online supplemental figure 3D–E). A pooled cohort analysis confirmed that MSLN expression was an independent prognostic factor for OS in patients with HGSOC (online supplemental figure 3F). Given the role of MSLN in cancer progression, we explored the potential role of MSLN in immune evasion. The Tumor Immune Dysfunction and Exclusion (TIDE) score predicts immune evasion and ICB therapy resistance.[19] In TCGA (The Cancer Genome Atlas) cohort, high *MSLN* expression was significantly associated with an increased TIDE score (online supplemental figure 3G). These findings highlight the dual role of MSLN as both a prognostic biomarker and a critical target in HGSOC management.

MSLN exhibits an inverse correlation with response to anti-PD-1 treatment in HGSOC organoids

The efficacy of ICB therapy in ovarian cancer remains limited, with response rates to anti-PD-1 monotherapy rarely exceeding 15%.[20 21] This underscores the urgent need for novel therapeutic targets to enhance ICB sensitivity. In mesothelioma, combining the MSLN-targeting immunotoxin LMB-100 with anti-PD-1 therapy significantly increased response rates from below 20% to nearly 40%, achieving substantial tumor regression.[7] Building on this evidence, we explored the role of MSLN in modulating anti-PD-1 efficacy in HGSOC. Using organoids derived from tissues of 28 patients with HGSOC, none of whom had received any prior treatments, including immunotherapies such as anti-PD-1. Based on their ex vivo response to anti-PD-1, the organoids were classified into two subgroups: responders (n=6), which exhibited marked immune marker alterations, and non-responders (n=22), which showed minimal changes(figure 1A). Notably, non-responders had a significantly higher MSLN H-score compared with responders (figure 1B, online supplemental figure 4A). During ex vivo experiments, anti-PD-1 was directly added to the organoid cultures. PD-1 blockade significantly promoted $CD8^+$ T-cell proliferation and cytotoxicity in organoids with low MSLN expression, whereas this effect was absent in those with high MSLN expression (figure 1C–1D, online supplemental figure 4B). These findings suggested that MSLN expression contributes to resistance to anti-PD-1 therapy. To further investigate this, we treated 22 non-responsive organoids with a combination of anti-PD-1 and LMB-100 antibodies. Positive responses were observed in 12 cases, predominantly in samples with high MSLN expression (figure 1E, online supplemental figure 4C). Immune profiling revealed distinct differences in $CD8^+$ T cells and TAMs populations between responders and non-responders (figure 1F, online supplemental figure 4D). In responders, TAMs were located closer to tumor cells and exhibited antitumorigenic phenotypes, while non-responders showed a predominance of protumorigenic TAMs (figure 1G–1J). Combination treatment significantly enhanced effector $CD8^+$ T-cell responses and promoted the polarization of antitumorigenic TAMs, characterized by high expression of HLA-DR, CD86 and CXCL9, while simultaneously reducing the prevalence of protumorigenic TAMs, defined by elevated levels of arginase-1 and CD206, as assessed by flow cytometry (figure 1K–1L). However, this trend was not observed in non-responsive samples (online supplemental figure 4E,F). These findings demonstrate that targeting MSLN, in conjunction with PD-1 blockade, represents a promising strategy to modulate the TME and overcome ICB resistance in HGSOC with higher MSLN expression.

Msln knockdown correlates with an antitumorigenic TME and confers protection against tumor development

We used single-cell RNA sequencing (scRNA-seq) data to analyze TME in HGSOC, with *MSLN* expression in the upper and lower quartiles. Tumors in the *MSLN*-low group exhibited a higher abundance of TAMs, with an enrichment of antitumorigenic subtypes and a reduced presence of protumorigenic subtypes (online supplemental figure 5A–E). Additionally, analysis of $CD8^+$ T-cell subtypes in the *MSLN*-low subgroup revealed increased levels of effector $CD8^+$ T cells, along with a lower prevalence of exhausted $CD8^+$ T cells (online supplemental figure 5F,G). Immunohistochemistry analysis of the Discovery cohort confirmed that low MSLN expression was associated with significantly higher levels of $CD8^+$ T cells and antitumorigenic TAMs ($CXCL9^+$ $CD68^+$), while showing lower expression of immune checkpoint molecules (cytotoxic T lymphocyte associate protein-4, T-cell immunoglobulin domain and mucin domain-3) and protumorigenic TAMs ($SPP1^+$ $CD68^+$) (online supplemental figures 6,7A). These findings were further corroborated by flow cytometric analysis of fresh tumors from patients with HGSOC (figure 2A).

To explore the functional impact of *Msln* knockdown, we generated stable *Msln* knockdown cell lines ($Msln^{KD}$). The knockdown efficacy was confirmed by a significant reduction in MSLN expression (online supplemental figure 7B–E). Colony formation and proliferation assays indicated that *Msln* knockdown significantly reduced proliferation, with a more pronounced effect observed in OV2944-HM1 cells (online supplemental figure 8A–D). The result of the western blot further confirmed that the secretion levels of MSLN were also significantly reduced in knockdown sequences #1 and #2 (online supplemental figure 8E). Initial in vivo studies demonstrated that stable Msln knockdown in OV2944-HM1 cells resulted in a complete loss of tumorigenic potential. However, due to the inherently low aggressiveness of OV2944-HM1 cells, we transitioned to using the ID8agg subline for subsequent in vivo experiments. The ID8agg subline was developed by serial passage of standard ID8 cells through immunocompetent wild-type hosts,[22] resulting in a highly aggressive ovarian cancer model. Compared with the standard ID8 model, ID8agg exhibits significantly enhanced tumorigenic potential, characterized by accelerated tumor growth and increased metastatic capacity.[23] Additionally, ID8agg reliably induces extensive peritoneal tumors resembling stage III and IV ovarian cancer, accompanied by a high incidence of hemorrhagic ascites, a hallmark of advanced HGSOC. These characteristics render ID8agg a more clinically relevant and robust platform for studying disease progression and evaluating therapeutic strategies. Using the ID8agg subcutaneous xenograft mouse model, we found that Msln knockdown ($Msln^{KD}$) cells significantly suppressed tumor growth in vivo (figure 2B). RNA sequencing of tumor tissues further revealed downregulation of key protumorigenic pathways, including members of the Wnt and Tgf-β families (figure 2C), suggesting that Msln plays a crucial role in driving tumor progression and maintaining a protumorigenic microenvironment. Additionally, protumorigenic pathways, such as Wnt, ERBB2-EGFR, Notch, and TGF-β, as well as pathways inhibiting

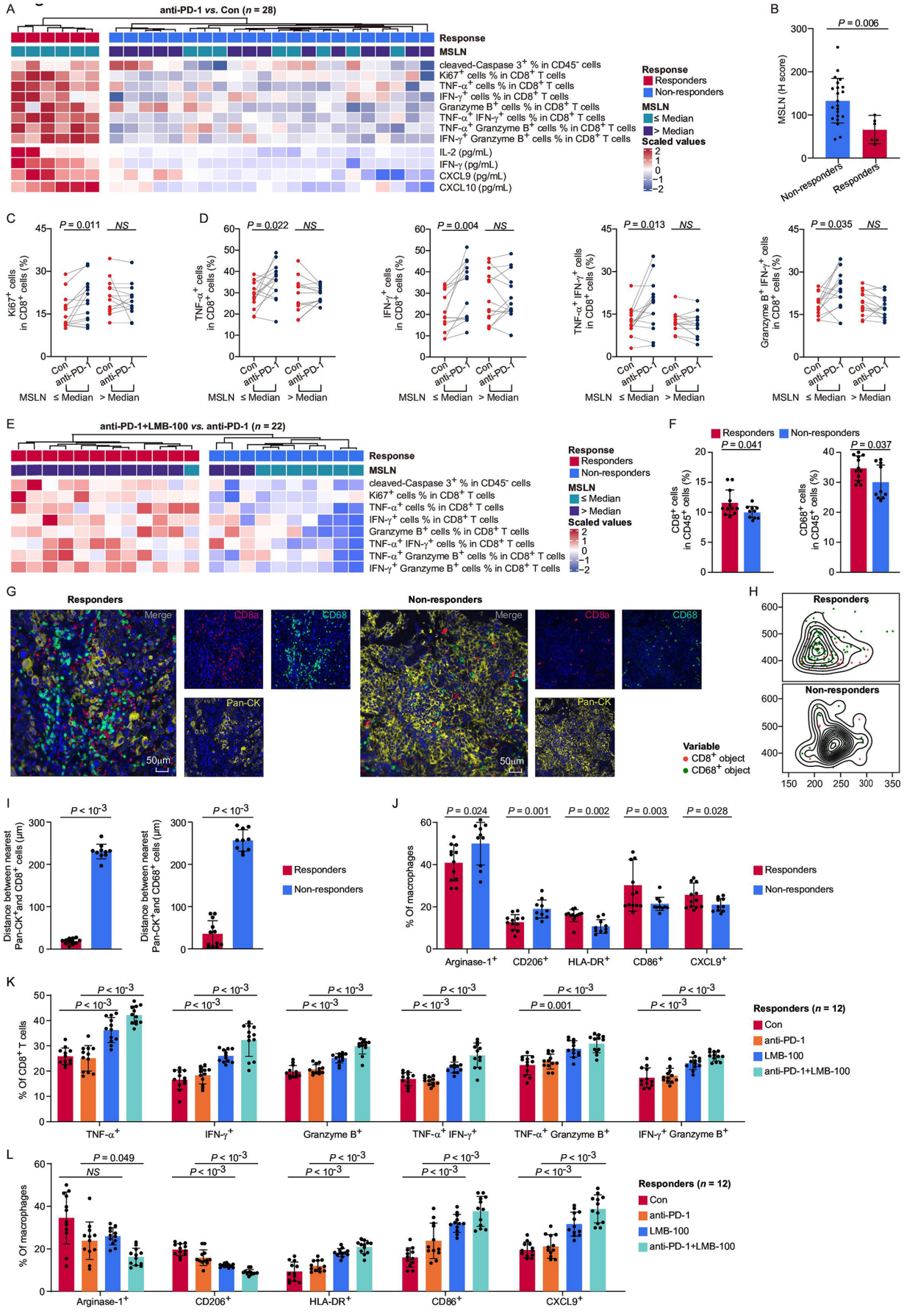

Figure 1 (Continued)

Figure 1 MSLN exhibits an inverse correlation with response to anti-PD-1 treatment in HGSOC organoids. (A) Heatmap clustering based on the relative abundance of cleaved caspase-3$^+$ CD45$^-$ cells, multiple subsets of CD8$^+$ T cells, TH1 cytokines (IL-2, IFN-γ) and TH1 chemokines (CXCL9, CXCL10) demonstrated anti-PD-1 responses in HGSOC organoids via flow cytometry (n=28). Color codes represent response subgroups, MSLN subgroups, and Z-score (log_2 intensity). Complete linkage and Euclidean distance were used for clustering. (B) MSLN expression levels, as indicated by the H-score, in anti-PD-1 responders (n=6) and non-responders (n=22) from HGSOC organoids. (C–D) Proportion of Ki-67 (C) and TNF-α, IFN-γ, TNF-α/IFN-γ, granzyme B/IFN-γ expressing CD8$^+$ T cells (D) in HGSOC organoids stratified by the median H-score of MSLN with isotype or anti-PD-1 treatment (n=28). (E) Heatmap clustering based on the relative abundance of cleaved caspase-3$^+$ CD45$^-$ cells and multiple subsets of CD8$^+$ T cells illustrating the response to the combination of anti-PD-1 and LMB-100 versus anti-PD-1 alone in HGSOC organoids, as determined by flow cytometry (n=22). Color codes represent response subgroups, MSLN subgroups, and Z-score (log_2 intensity). Complete linkage and Euclidean distance were used for clustering. (F) The proportion of CD8$^+$ and CD68$^+$ cells among CD45$^+$ cells in HGSOC organoids between responders (n=12) and non-responders (n=10) to the combination of anti-PD-1 and LMB-100 treatment. (G–H) Representative immunofluorescence images (G) and contour maps (H) illustrating CD68, CD8a, and Pan keratin staining in responders and non-responders to the combination of anti-PD-1 and LMB-100 treatment. (I) Quantification of the distance from CD8$^+$ T cells (left) and CD68$^+$ macrophages (right) to the nearest Pan keratin$^+$ cell in responders (n=12) and non-responders (n=10) to anti-PD-1+LMB-100 treatment. (J) Proportion of arginase-1, CD206, HLA-DR, CD86, CXCL9 expressing CD68$^+$ macrophages in HGSOC organoids between responders (n=12) and non-responders (n=10) to anti-PD-1+LMB-100 treatment. (K–L) Proportion of TNF-α, IFN-γ, granzyme B, TNF-α/IFN-γ, TNF-α/granzyme B, and IFN-γ/granzyme B expressing CD8$^+$ T cells (K) and arginase-1, CD206, HLA-DR, CD86, CXCL9 expressing CD68$^+$ macrophages (L) in HGSOC organoids under the treatment with isotype IgG, anti-PD-1, LMB-100 alone, or the combination of anti-PD-1 and LMB-100 for 48 hours (n=12), as assessed by flow cytometry. Data are presented as mean±SD. Statistical significance was determined using a two-tailed unpaired Student's t-test or Mann-Whitney U test (B, F, I–J), two-sided paired Student's t-test (C–D), and two-way analysis of variance, followed by Tukey's post hoc test for multiple comparisons (K–L). Con, control; CXCL9, C-X-C motif chemokine ligand 9; CXCL10, C-X-C motif chemokine ligand 10; HGSOC, high-grade serous ovarian cancer; IFN-γ, interferon-γ; IL-2, interleukin-2; MSLN, mesothelin; NS, no significant difference; Pan-CK, pan cytokeratin; PD-1, programmed cell death protein-1; TNF-α, tumor necrosis factor-α.

T-cell proliferation, were significantly downregulated in Msln^{KD} tumors (figure 2D–2E). In contrast, the T cell-inflamed gene expression profile was activated in Msln^{KD} tumors (figure 2F).

Using an orthotopic ovarian tumor model, we demonstrated that *Msln* knockdown significantly delayed tumor progression (online supplemental figure 8F,G), inhibited peritoneal metastasis expansion (figure 2G–2H), and extended OS in intraperitoneal exnograft mice (figure 2I). Post-mortem analysis revealed reduced hemorrhagic ascites and fewer secondary tumor foci in the Msln^{KD} group (online supplemental figure 8H,I). Furthermore, *Msln* knockdown enhanced effector CD8$^+$ T cells infiltration and antitumorigenic TAM populations while reducing protumorigenic TAMs (figure 2J–2K, online supplemental figure 8J–L). To confirm that the tumor-suppressive effects of *Msln* knockdown were mediated by CD8$^+$ T cells and TAMs, we performed depletion experiments in an intraperitoneal tumor-bearing mouse model (online supplemental figures 9,10A–C). CD8$^+$ T cells depletion abolished the tumor-suppressive effects of *Msln* knockdown, leading to accelerated tumor growth, increased hemorrhagic ascites, and recurrence of metastatic lesions (figure 2L–2N). Similarly, macrophage depletion nullified the inhibitory effects of *Msln* knockdown on tumor growth, ascitic fluid formation, and metastasis (figure 2O–2Q). Flow cytometric analysis of the ascitic TME in macrophage-depleted mice revealed a significant reduction in effector CD8$^+$ T-cell infiltration (figure 2R, online supplemental figure 10D), underscoring the critical role of macrophages in enabling CD8$^+$ T cells mediated antitumor activity induced by *Msln* knockdown.

MSLN augments protumorigenic macrophage polarization in a CD24-dependent manner

To explore the mechanisms by which MSLN mediates TAM's polarization, we employed flow cytometry to analyze BMDMs co-cultured with tumor cells in both direct and indirect contact setups. The polarization of TAMs occurred exclusively in the direct co-culture system, where Msln^{KD} promoted a shift towards an antitumorigenic phenotype (figure 3A, online supplemental figure 11). Since this effect was observed only under direct cell–cell interactions, we focused on membrane surface molecules that potentially drive this process. Using overlapping analyses of DEGs from bulk RNA sequencing and scRNA-seq data sets (figure 3B), we identified CD24 as the most significantly altered surface molecule associated with macrophage polarization.[24] *Msln* knockdown reduced CD24 expression, an effect that could be reversed by treatment with recombinant MSLN (rMSLN; figure 3C–3D). This positive correlation between MSLN and CD24 expression was further validated in HGSOC cohorts (figure 3E, online supplemental figure 12A–C). Based on these observations, we hypothesized that CD24 mediates MSLN-induced TAM polarization. To test this, we generated a CD24 overexpressing ID8agg cell line (figure 3F–3G). Co-culture experiments demonstrated that CD24 overexpression reversed the antitumor polarization of TAMs induced by Msln^{KD} cells (figure 3H). Additionally, CD24 overexpression suppressed the enhanced phagocytic capacity of TAMs observed in the presence of Msln^{KD} cells (figure 3I and online supplemental figure 12D). Notably, CD24 overexpression rescued the inhibitory effects of Msln^{KD}

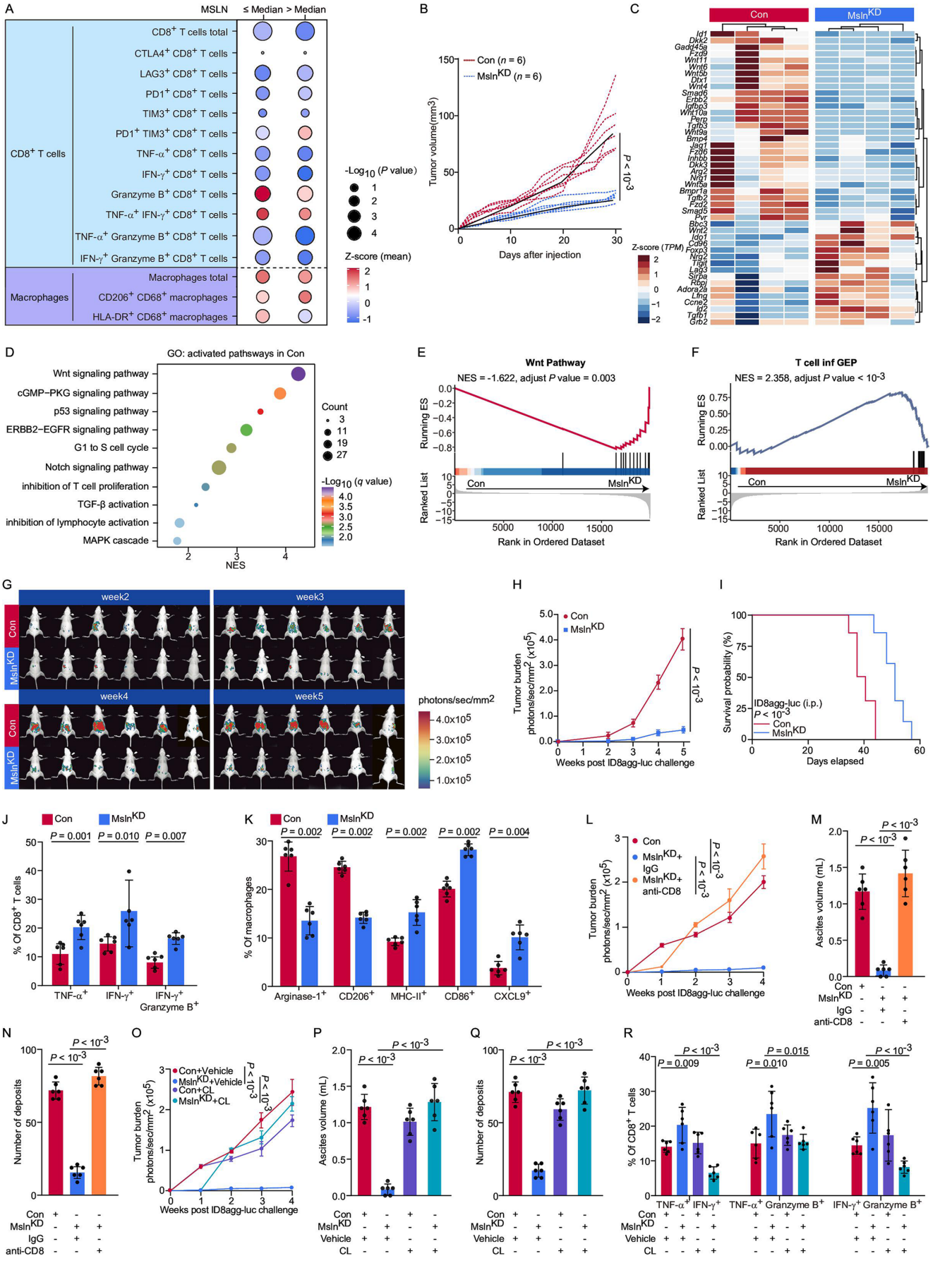

Figure 2 (Continued)

Figure 2 *Msln* knockdown correlates with an antitumorigenic TME and confers protection against tumor development. (A) Dot plots demonstrating the abundance of $CD8^+$ T-cell subsets and polarized TAMs between the $MSLN^{low}$ (n=24) and $MSLN^{high}$ (n=24) subgroups in patients with HGSOC. Dot size represents $-\log_{10}$(p value), while the color scale indicates z-score normalized immune cell abundance, as evaluated by flow cytometry. (B) Tumor growth trajectories in immunocompetent C57BL/6 mice following subcutaneous administration of 5×10^6 ID8agg-control cells or ID8agg-$Msln^{KD}$ cells (n=6 per group). The dashed lines depict individual mice, whereas the solid line represents the mean tumor volume. (C) Heatmap illustrating DEGs between subcutaneous tumor tissues from control and $Msln^{KD}$ groups, based on bulk RNA sequencing analysis. The bars on the right represent the z-scores of TPM for the corresponding genes. (D) GSEA (GO biological processes) on genes ranked by $\log_2$ (fold change) between control and $Msln^{KD}$ group. Bars on the right indicate the range of $-\log_{10}$ (q value) of corresponding pathways. Dots on the right represent the number of counts. Norminal q values were adjusted using the Benjamini-Hochberg method. (E–F) GSEA revealed enrichment of the Wnt pathway (E) and the T-cell infiltration gene expression profile (T cell inf gene expression profile) pathway (F) on *Msln* knockdown, compared with the control. The nominal p value was adjusted using the Benjamini-Hochberg method. (G–I) For the advanced ovarian cancer model, ID8agg-luc cells with or without *Msln* knockdown were implanted via intraperitoneal injection (n=6 per group). The experiment was conducted with two independent biological replicates. (G) IVIS bioluminescent images of peritoneal tumor burden from week 2 to week 5 after control or $Msln^{KD}$ ID8agg-luc cell injection. (H) Quantification of the tumor burden in mice shown in (G) via radiant efficiency. (I) Kaplan-Meier survival plot of mice corresponding to (G). (J–K) Proportion of TNF-α, IFN-γ, IFN-γ/granzyme B expressing $CD8^+$ T cells (J) and arginase-1, CD206, MHC-II, CD86, CXCL9 expressing $F4/80^+$ $CD11b^+$ cells (K) from ascites of mice corresponding to (G) (n=6 per group). (L–N) To evaluate the role of $CD8^+$ T cells in advanced ovarian cancer, ID8agg-luc cells with or without *Msln* knockdown were implanted via intraperitoneal injection in mice with or without depletion of $CD8^+$ T cells (n=6 per group). Tumor burden was quantified by evaluating fluorescence via radiant efficiency (L), ascites volume (M), and metastatic nodules in the peritoneal wall, omentum, mesentery, and diaphragm (N). (O–Q) To evaluate the role of macrophages in advanced ovarian cancer, ID8agg-luc cells with or without *Msln* knockdown were intraperitoneally injected into mice with or without macrophage depletion (n=6 per group). Tumor burden was quantified by evaluating fluorescence via radiant efficiency (O), ascites volume (P), and metastatic nodules in the peritoneal wall, omentum, mesentery, and diaphragm (Q). (R) Proportion of TNF-α/IFN-γ, TNF-α/granzyme B, and IFN-γ/granzyme B expressing $CD8^+$ T cells from ascites of mice corresponding to (O). Data are presented as mean±SD. Statistical significance was assessed using two-tailed unpaired Student's t-test or Mann-Whitney U test (J–K), log-rank test (I), and two-way analysis of variance, followed by Tukey's post hoc test for multiple comparisons (H, L–R). CL, clodronate liposomes; Con, control; CTLA-4, cytotoxic T lymphocyte associate protein-4; CXCL9, C-X-C motif chemokine ligand 9; DEGs, differentially expressed genes; GO, Gene Ontology; GSEA, Gene Set Enrichment Analysis; HGSOC, high-grade serous ovarian cancer; IVIS, In Vivo Imaging System; IFN-γ, interferon-γ; IgG, immunoglobulin G; KD, knockdown; LAG3, lymphocyte activation gene-3; *Msln*, mesothelin; NES, normalized enrichment score; PD-1, programmed cell death-1; TAMs, tumor-associated macrophages; TIM-3, T-cell immunoglobulin domain and mucin domain-3; TME, tumor microenvironment; TNF-α, tumor necrosis factor-α; TPM, transcripts per million.

cells on $CD8^+$ T cells proliferation and cytotoxic activities (figure 3J–3L, online supplemental figure 12E,F). The gating strategies for flow cytometry analyses of in vitro macrophage phagocytosis of tumor cells and T-cell proliferation assay are detailed in online supplemental figures 13,14. These results identify CD24 as a critical mediator of MSLN-induced TAMs polarization. This previously unrecognized CD24-dependent mechanism highlights a pathway by which high MSLN expression fosters immune evasion of HGSOC.

MSLN induces CD24 expression through Wnt signaling

To elucidate the mechanisms by which MSLN modulates CD24 expression, we analyzed overlapping pathway activities, including Wnt and NF-κB signaling, using bulk RNA sequencing data from subcutaneous tumors and ID8agg cells with or without *Msln* knockdown, as well as scRNA-seq data from HGSOC samples with $MSLN^+$ cancer cells versus $MSLN^-$ cancer cells (figure 4A). To investigate the role of these pathways in MSLN-induced CD24 expression, we treated cells with Wnt signaling inhibitor ICG-001 and NF-κB inhibitor JSH-23. Notably, ICG-001 significantly suppressed CD24 expression induced by rMSLN (figure 4B–4D). Consistently, activation of the Wnt pathway using the agonist BML-284 markedly enhanced CD24 expression in ID8agg cells (figure 4E–4G). As canonical Wnt signaling involves β-catenin nuclear translocation,[25] we observed that rMSLN increased levels of active β-catenin (figure 4H) and facilitated its nuclear translocation (figure 4I–4J). Interestingly, our findings suggest that Wnt/β-catenin pathway activated by MSLN establishes a self-reinforcing loop that amplifies MSLN transcription (figure 4K). To further investigate the interaction between Wnt signaling and the CD24 promoter, luciferase reporter assays were conducted in ID8agg cells. Treatment with rMSLN rescued CD24 luciferase activity in $Msln^{KD}$ cells, an effect that was inhibited by Wnt signaling blockade (figure 4L). Sequence analysis of 2.0 kb upstream region of the transcriptional start site of the mouse *Cd24a* gene identified putative *Tcf3* and *Tcf7* binding motif. Truncation experiments using CD24 promoter deletion constructs revealed that deletion of the −1,169 to 0 bp region significantly reduced rMSLN-mediated luciferase activation, indicating that this segment, which includes *the Tcf7* responsive element, is the primary site for Wnt signaling-mediated CD24 transcriptional activation. Subsequently, a *Tcf7* point mutation was introduced into the CD24 plasmid, which also resulted in a significant reduction in rMSLN-mediated luciferase activity (figure 4M).

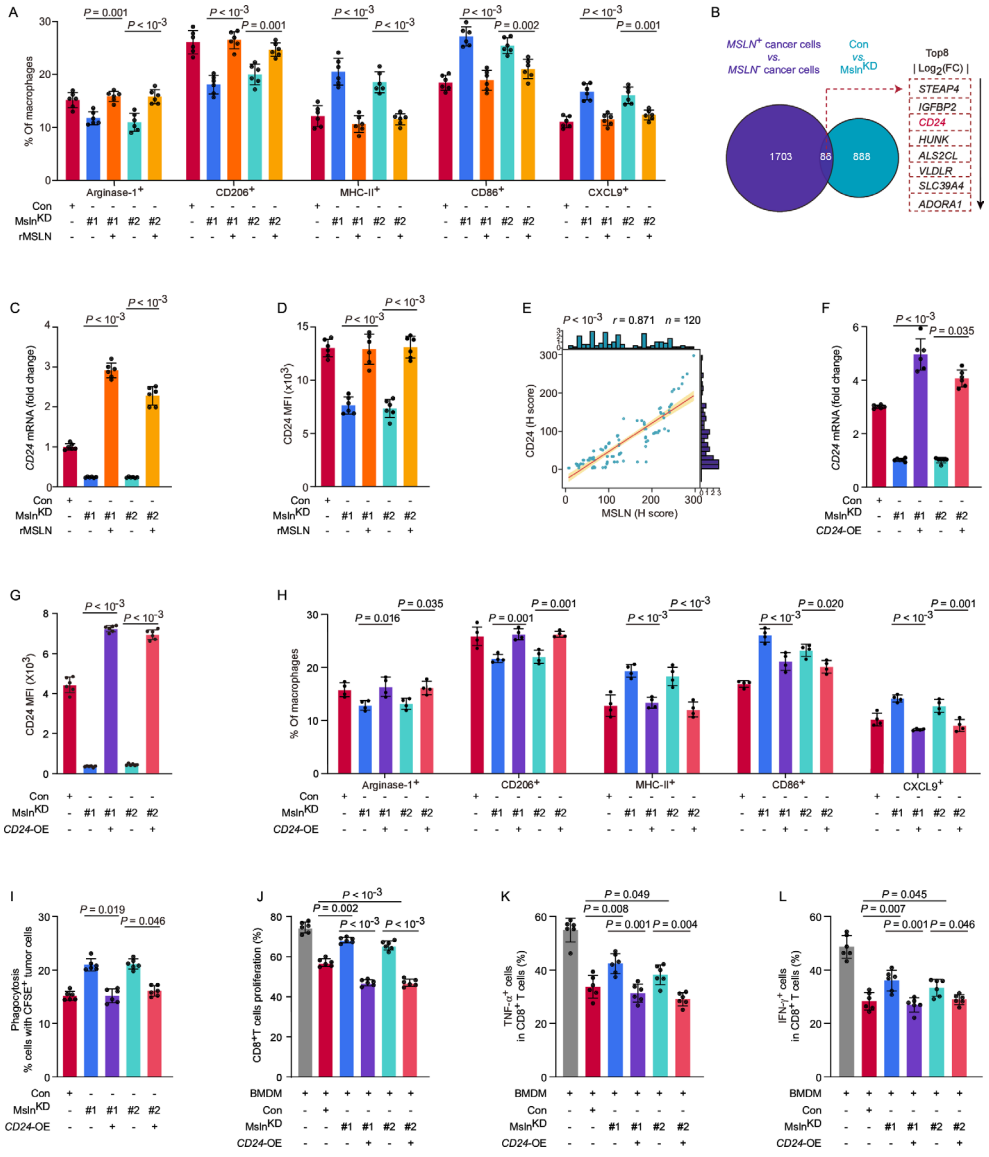

Figure 3 MSLN augments protumorigenic macrophage polarization in a CD24-dependent manner. (A) The proportion of F4/80$^+$ CD11b$^+$ cells expressing Arginase-1, CD206, MHC-II, CD86, or CXCL9 in a direct co-culture system. BMDMs were co-cultured with either control or Msln^{KD} ID8agg cells, with or without supplementary rMSLN for 48 hours (n=6 per group). The experiment was conducted with three independent biological replicates. (B) Venn diagram summarizing the number of DEGs (p adj≤0.05). The left circle represents the number of DEGs between *MSLN*$^+$ and *MSLN*$^-$ cancer cells from scRNA-seq of HGSOC in GSE180661. The right circle represents the number of DEGs between control and Msln^{KD} ID8agg cells. The top eight overlapping DEGs in each analysis, ranked in descending order by $\log_2$(FC), are enumerated on the right. (C–D) Relative mRNA expression of *Cd24a* (C) and MFI of CD24 (D) in control or Msln^{KD} ID8agg cells in the absence or presence of rMSLN for 24 hours (n=6 per group). The experiment was conducted with three independent biological replicates. (E) Positive correlation between the IHC score of MSLN and CD24 protein in HGSOC from the Discovery cohort (n=120). (F–G) Relative mRNA expression of *Cd24a* (F) and MFI of CD24 (G) in control or Msln^{KD} ID8agg cells with or without CD24 overexpression (n=6 per group). The experiment was conducted with three independent biological replicates. (H–I) Proportion of arginase-1, CD206, MHC-II, CD86, CXCL9 expressing F4/80$^+$ CD11b$^+$ (H), and phagocytosis of BMDMs (I) in direct co-culture between BMDMs and control or Msln^{KD} ID8agg cells with or without CD24 overexpression for 48 hours (n=6 per group). (J–L) The proliferation of CD8$^+$ T cells was assessed via CFSE dilution (J), and the expression of TNF-α (K) and IFN-γ (L) in CD8$^+$ T cells was evaluated by direct co-culture of CD8$^+$ T cells and BMDMs pre-cultured with control or Msln^{KD} ID8agg cells in the absence or presence of CD24 overexpression for 48 hours (n=6 per group). Data are presented as mean±SD. Statistical significance was determined by two-way analysis of variance followed by Tukey's post hoc test for multiple comparisons (A, C–D, J–L), Spearman's correlation (E), and the Kruskal-Wallis test with Dunn's post hoc test for multiple comparisons (F–I). BMDMs, bone marrow-derived macrophages; CFSE, carboxyfluorescein succinimidyl ester; Con, control; CXCL9, C-X-C motif chemokine ligand 9; DEGs, differentially expressed genes; FC, fold change; HGSOC, high-grade serous ovarian cancer; IFN-γ, interferon-γ; IHC, immunohistochemistry; KD, knockdown; MFI, median fluorescence intensity; mRNA, messenger RNA; MSLN, mesothelin; OE, over expression; p adj, adjusted p value; rMSLN, recombinant mesothelin; scRNA-seq, single-cell RNA sequencing; TNF-α, tumor necrosis factor-α.

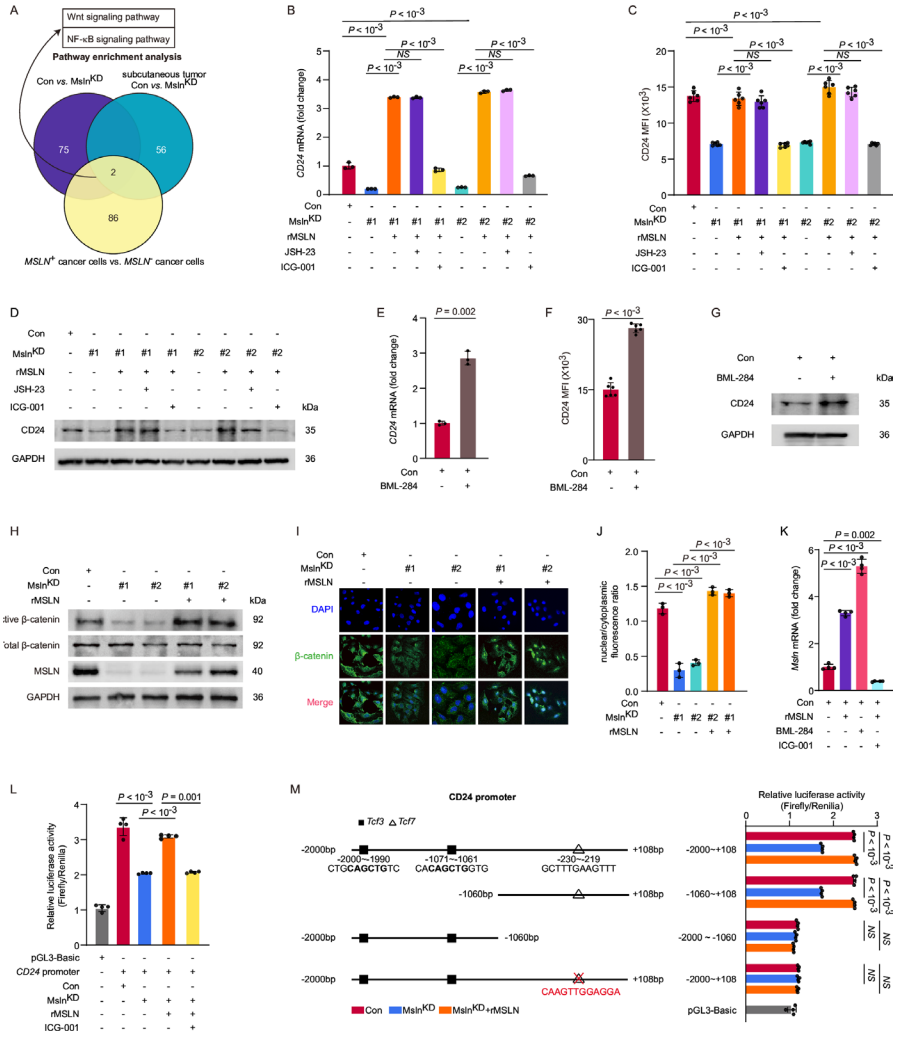

Figure 4 MSLN induces CD24 expression through Wnt signaling. (A) Venn diagram illustrating overlapping enrichment pathways between functional enrichment analysis for GO, KEGG and Wiki pathways (with Benjamini-Hochberg-adjusted p value≤0.05) using significantly upregulated DEGs (p≤0.05, $\log_2$ (fold change) ≥1) from the bulk transcriptomic comparison of control and Msln^{KD} ID8agg cells, comparison of *MSLN*$^{+}$ with *MSLN*$^{-}$ cancer cells from scRNA-seq of HGSOC in GSE180661 and comparison of bulk transcriptomic comparison of control and Msln^{KD} subcutaneous tumor tissues. Two pathways associated with CD24 are listed above. (B–C) Relative mRNA expression of *Cd24a* (B, n=3 per group) and MFI of CD24 (C, n=6 per group) in control or Msln^{KD} ID8agg cells in the absence or presence of rMSLN, which were pretreated with NF-κB pathway inhibitor (JSH-23) or Wnt pathway inhibitor (ICG-001) for 24 hours. The experiment was conducted with three independent biological replicates. (D) Comparison of levels of CD24 in control or Msln^{KD} ID8agg cells in the absence or presence of rMSLN, which were pretreated with NF-κB pathway inhibitor (JSH-23) or Wnt pathway inhibitor (ICG-001) for 24 hours. GAPDH served as an internal control. (E–F) Relative mRNA expression of *Cd24a* (E, n=3 per group) and MFI of CD24 (F, n=6 per group) in control ID8agg cells with or without treatment with a Wnt pathway agonist (BML-284) for 24 hours. The experiment was conducted with three independent biological replicates. (G) Comparison of levels of CD24 in control ID8agg cells with or without treatment with a Wnt pathway agonist (BML-284) for 24 hours. GAPDH served as an internal control. (H) Comparison of levels of dephosphorylated β-catenin (active β-catenin) and total β-catenin in control and Msln^{KD} ID8agg cells with or without rMSLN exposure for 24 hours. GAPDH served as an internal control. (I–J) Representative immunofluorescence images (I) and quantification of nuclear/cytoplasmic fluorescence ratio (J) illustrating the location of β-catenin (green) in control or Msln^{KD} ID8agg cells in the absence or presence of rMSLN. (K) Bar plot illustrating relative mRNA levels of *Msln* in ID8agg cells (n=4 per group) with or without the addition of rMSLN, BML-284 and ICG-001. (L) Luciferase reporter assays for control or Msln^{KD} ID8agg cells transfected with full-length *Cd24a* promoter-containing reporter plasmids with or without rMSLN and ICG-001 treatment (n=4 per group). (M) Luciferase reporter assays for control or Msln^{KD} ID8agg cells transfected with specified reporter plasmids containing either full-length, truncated *Cd24a* promoters or *Tcf7* point mutated *Cd24a* promoters (n=4 per group). Data are shown as mean±SD. Statistical significance was assessed using two-way analysis of variance, followed by Tukey's post hoc test for multiple comparisons (B–C, J–L), two-tailed unpaired Mann-Whitney U test (E–F) and the Kruskal-Wallis test with Dunn's post hoc test for multiple comparisons (M). Con, control; DAPI, 4',6-diamidino-2-phenylindole; DEGs, differentially expressed genes; GO, Gene Ontology; HGSOC, high-grade serous ovarian cancer; KD, knockdown; KEGG, Kyoto Encyclopedia of Genes and Genomes; MFI, median fluorescence intensity; RNA, messenger RNA; MSLN, mesothelin; NS, no significant difference; rMSLN, recombinant mesothelin; scRNA-seq, single-cell RNA sequencing.

MSLN facilitates immune evasion in ovarian cancer through the CD24/Siglec-10 interaction

The CD24/Siglec-10 signaling axis is a critical mechanism of immune evasion, facilitating communication between cancer cells and TAMs. This interaction suppresses TAMs-mediated phagocytosis of malignant cells, thereby promoting tumor progression.[24] Analysis of scRNA-seq data from HGSOC revealed that *SIGLEC-10*$^{+}$ TAMs exhibit a protumorigenic profile, characterized by increased expression of markers such as *SPP1*, *CD163*, *FCGR2A*, *FCGR2B*, *FN1* and *TREM2* (figure 5A). GSEA further demonstrated that *SIGLEC-10*$^{+}$ TAMs in the *MSLN*-Low expression group exhibited significantly enhanced phagocytic and antigen-presenting capabilities (figure 5B). To validate these findings, flow cytometry analysis of Siglec-10^{+} TAMs from 22 patients with HGSOC was performed. In HGSOC with high MSLN expression, Siglec-10^{+} TAMs displayed a protumorigenic phenotype, marked by increased levels of arginase-1 and CD206, and reduced levels of HLA-DR, CD86, and CXCL9 (figure 5C). Co-culture experiments further revealed that CD24 overexpression reversed the antitumorigenic polarization of TAMs induced by *Msln* knockdown (figure 5D). Consistently, in an intraperitoneal ID8agg mouse model, CD24 overexpression restored tumor progression in Msln^{KD} cells, reduced survival times, and increased hemorrhagic ascites and secondary metastatic foci (figure 5E–5H). Moreover, CD24 overexpression inhibited the cytotoxic activity of CD8^{+} T cells in ascites from the Msln^{KD} group (figure 5I) and reversed the antitumorigenic polarization induced by *Msln* knockdown in TAMs (figure 5J). Finally, the clinical significance of the co-expression of CD24 and MSLN was examined. Low CD24 expression effectively negated the poor prognosis associated with high MSLN levels, while patients with high CD24 and high MSLN expression demonstrated the lowest median survival (figure 5K, log-rank p value=0.002, median survival 44 months vs 36 months). These findings underscore the role of CD24 in neutralizing the antitumor benefits of *Msln* knockdown and further highlight its potential as a therapeutic target for overcoming immune evasion mechanisms in HGSOC.

Msln knockdown synergize with anti-PD-1 immunotherapy in vivo

Given that *Msln* knockdown reprograms the immunosuppressive TME, we hypothesized that it would enhance the efficacy of anti-PD-1 immunotherapy in vivo. The workflow of the in vivo experiment is illustrated in online supplemental figure 15A. In an intraperitoneal mouse model, *Msln* knockdown overcame anti-PD-1 resistance, resulting in substantial reductions in tumor growth (figure 6A–6B) and prolonged survival (figure 6C). Furthermore, the combination of *Msln* knockdown and anti-PD-1 treatment inhibited ascetic fluid formation and secondary metastases (figure 6D, online supplemental figure 15B,C). Next, we examined the effects of *Msln* knockdown combined with anti-PD-1 treatment on the tumor immune microenvironment. This combination led to enhanced activation of cytotoxic CD8^{+} T cells and a decreased abundance of Siglec-G^{+} TAMs, alongside polarization of antitumorigenic TAMs (figure 6E–6G, online supplemental figure 15D–F). Specifically, we observed an increase in Tpex, which proliferates and differentiates into intermediate (Tex-int) and terminally exhausted (Tex-term) cells, contributing to the ICB response.[26 27] Consistently, combination treatment increased the proportion of Tpex and Tex-int cells while reducing the fraction of Tex-term cells (figure 6H). We further assessed the effect of anti-PD-1 and LMB-100 monotherapies, as well as their combination, in HGSOC organoids. These treatments progressively reduced CD24 expression in tumor cells (figure 6I) and polarized antitumorigenic TAMs (figure 6J). The induction of antitumor immune memory is crucial for enabling the immune system to mount a swift and effective response against previously encountered tumor antigens.[28] To evaluate immune memory, we performed a rechallenge experiment using Msln^{KD} ID8agg cells with anti-PD-1 treatment. 60 days after the final IVIS assessment, the rechallenged mice showed minimal tumor progression and extended survival (figure 6K–6L). Flow cytometry confirmed that this combination treatment induced antitumor immune memory in a peritoneal mouse model (figure 6M). Notably, previous studies have shown that MSLN targeting can facilitate the formation of TLS in a humanized murine model.[8] In our study, the combination treatment significantly enhanced TLS formation, which was closely correlated with increased Tpex cell abundance (online supplemental figure 15G–I). These findings suggest that MSLN targeting, in combination with anti-PD-1 treatment, can improve responsiveness to anti-PD-1 immunotherapy by promoting antitumorigenic TAMs polarization, enhancing cytotoxic T-cell activity, and fostering TLS formation and Tpex cell proliferation.

DISCUSSION

This study elucidated the significant role of MSLN, a tumor-specific cell surface glycoprotein, in HGSOC (graphic abstract). The investigation revealed that MSLN, which is abundantly expressed in HGSOC, enhances CD24 expression through the activation of the Wnt/β-catenin signaling cascade. Furthermore, this study demonstrated that *Msln*-mediated activation of Wnt/β-catenin signaling creates a self-reinforcing loop that amplifies *Msln* transcription. Consequently, this process triggers the CD24/Siglec-10 axis, resulting in the inhibition of effector functions in both macrophages and CD8^{+} T cells within the TME. This mechanism ultimately facilitates immune evasion by ovarian cancer cells. These results suggest multiple avenues for potential translational applications. First, the expression levels of MSLN may serve as reliable indicators of poor prognosis in patients with HGSOC. Second, MSLN could serve as a valuable biomarker for predicting patient responses to

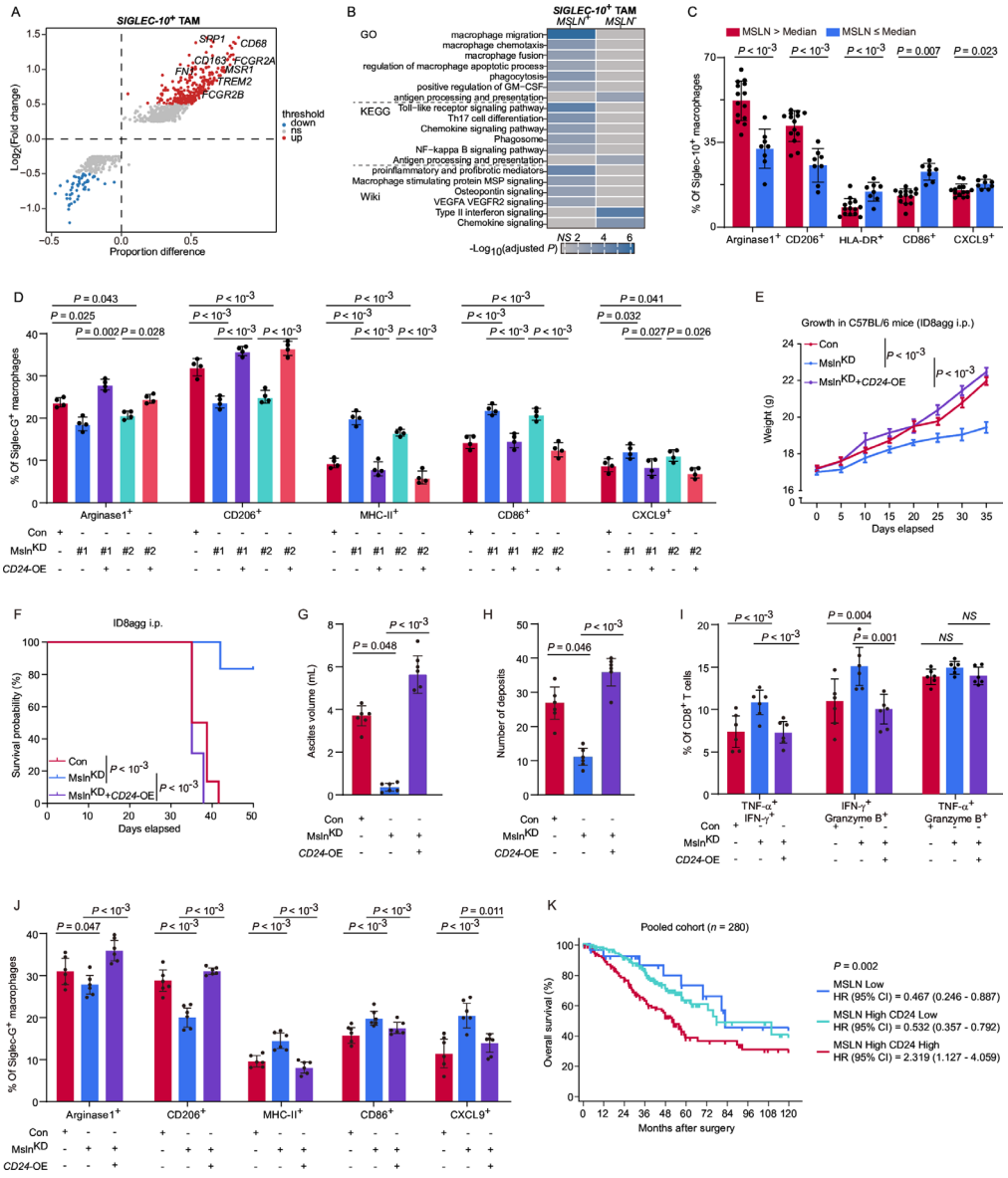

Figure 5 MSLN facilitates immune evasion in ovarian cancer through the CD24/Siglec-10 interaction. (A) Quadrant plot depicting DEGs identified in *SIGLEC-10*$^+$ TAMs and other cells (FDR q<0.05, $\log_2$(fold change) ≥1). (B) Heatmap showing enrichment scores (–$\log_{10}$(adjusted p values), Benjamini-Hochberg corrected FDR) of functional pathways in GO, KEGG and Wiki pathway databases using significant DEGs of *SIGLEC-10*$^+$ TAMs between high and low *MSLN* subgroups. (C) Relative abundance of arginase-1, CD206, HLA-DR, CD86 and CXCL9 expressing Siglec-10$^+$ cells within CD68$^+$ cells in single-cell suspension of tumor tissues from patients with HGSOC corresponding to figure 1E (n=22). (D) Relative abundance of arginase-1, CD206, MHC-II, CD86, and CXCL9 expressing Siglec-G$^+$ cells within F4/80$^+$ CD11b$^+$ cells, following 48-hour co-culture of BMDMs with control or Msln^{KD} ID8agg cells, with or without CD24 overexpression (n=4 per group). (E–F) Body weight trajectories (E) and Kaplan-Meier survival curves (F) of advanced ovarian cancer models intraperitoneally injected with control or Msln^{KD} ID8agg cells with or without CD24 overexpression (n=6 per group). (G–H) Quantification of ascites volume (G) and metastatic nodules (H) in the ovarian cancer models in (E) at the endpoint (n=6 per group). (I–J) Proportion of TNF-α/IFN-γ, IFN-γ/granzyme B and TNF-α/granzyme B expressing CD8$^+$ T cells (I) and arginase-1, CD206, MHC-II, CD86 and CXCL9 expressing Siglec-G$^+$ cells in F4/80$^+$ CD11b$^+$ cells (J) in ascites from ovarian cancer models in (E). (K) Kaplan-Meier plots depicting OS rates of patients with HGSOC from the Pooled cohort (n=280), stratified into three groups based on combined MSLN and CD24 expression: MSLN-low, MSLN-high/CD24-low, and MSLN-high/CD24-high. Data are shown as mean±SD. Statistical significance was determined by two-tailed unpaired Mann-Whitney U test (C), Kruskal-Wallis test with Dunn's post hoc test (D, G–J), two-way analysis of variance followed by Tukey's post hoc test for multiple comparisons (E), and log-rank test (F, K). BMDMs, bone marrow-derived macrophages; Con, control; CXCL9, C-X-C motif chemokine ligand 9; DEGs, differentially expressed genes; FDR, false discovery rate; GO, Gene Ontology; HGSOC, high-grade serous ovarian cancer; IFN-γ, interferon-γ; i.p., intraperitoneal injection; KD, knockdown; KEGG, Kyoto Encyclopedia of Genes and Genomes; MSLN, mesothelin; NS, no significant difference; OE, overexpression; OS, overall survival; Siglec-G, sialic acid-binding immunoglobulin-like lectin G; Siglec-10, sialic acid-binding immunoglobulin-like lectin 10; TAMs, tumor-associated macrophages; TNF-α, tumor necrosis factor-α.

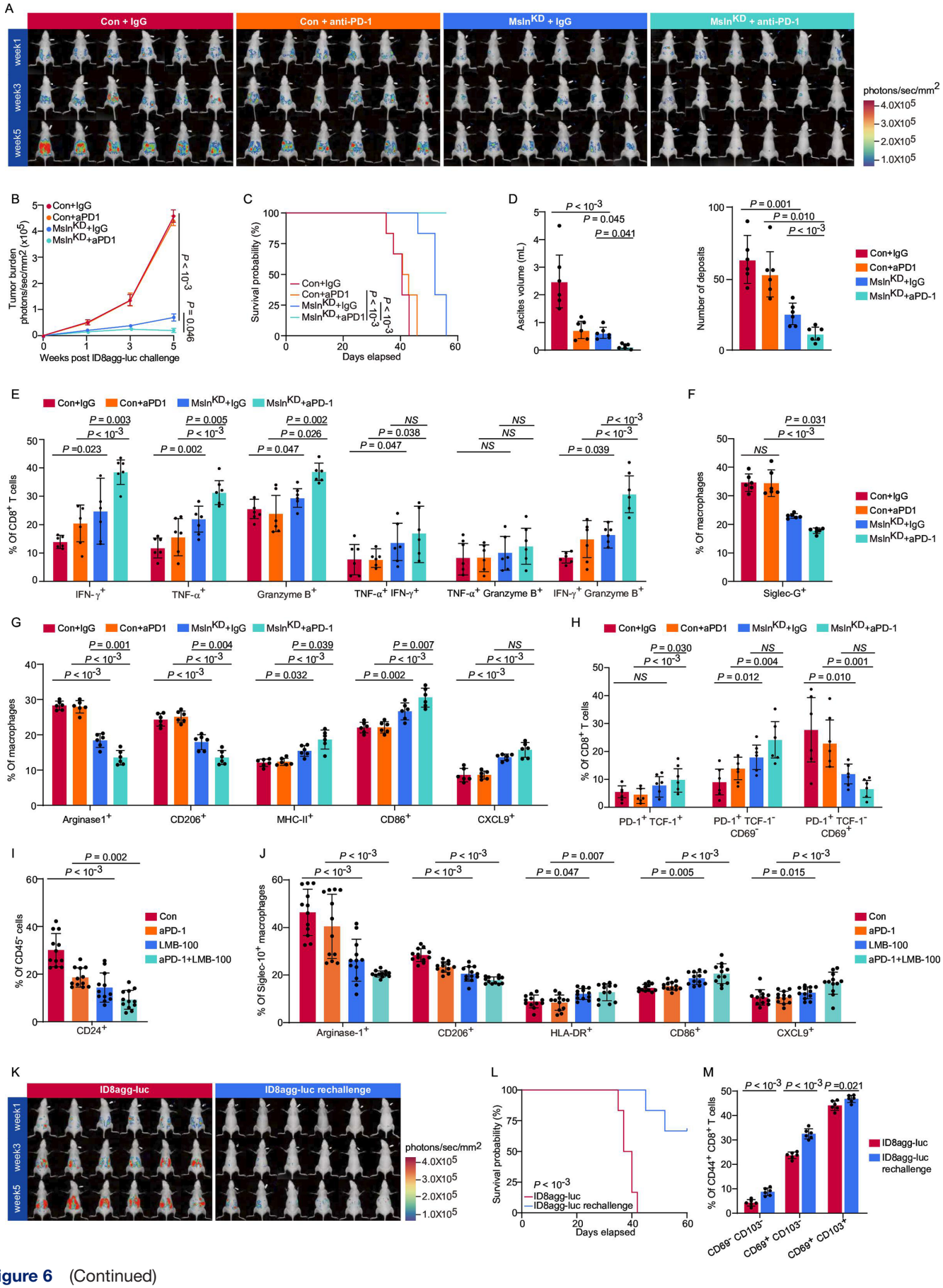

Figure 6 (Continued)

Figure 6 *Msln* knockdown synergize with anti-PD-1 immunotherapy in vivo. (A–B) Representative IVIS bioluminescent images (A) and mean photon flux (B) of the peritoneal tumor burden at weeks 1, 3, and 5 following the injection of control *or* $Msln^{KD}$ ID8agg-luc cells with anti-PD-1 treatment (n=6 per group). (C) Kaplan-Meier survival plot of mice corresponding to (A). (D) Quantification of ascites volume (left) and metastatic nodules (right) in the peritoneum, omentum, mesentery, and diaphragm of mice in (A). (E–G) Proportion of IFN-γ, TNF-α, granzyme B, TNF-α/IFN-γ, TNF-α/granzyme B, IFN-γ/granzyme B expressing $CD8^+$ T cells (E), Siglec-G expressing $F4/80^+$ $CD11b^+$ cells (F) and arginase-1, CD206, MHC-II, CD86 and CXCL9 expressing $F4/80^+$ $CD11b^+$ cells (G) in ascites of mice corresponding to (A). (H) Percentage of $PD\text{-}1^+$ $TCF\text{-}1^+$, $PD\text{-}1^+$ $TCF\text{-}1^-$ $CD69^-$, $PD\text{-}1^+$ $TCF\text{-}1^-$ $CD69^+$ $CD8^+$T cells in ascites of mice corresponding to (A). (I–J) Percentage of $CD24^+$ cells in $CD45^-$ cells (I) and arginase-1, CD206, HLA-DR, CD86, CXCL9 expressing $Siglec\text{-}10^+$ macrophages (J) in HGSOC organoids treated with IgG control, anti-PD-1, LMB-100 alone, or the combination of anti-PD-1 and LMB-100. (K–L) Representative bioluminescence images (K) and survival curve (L) of tumor cell rechallenge in mice treated and cured with the combination of $Msln^{KD}$ cells and anti-PD-1 treatment. A minimum of 60 days following the disappearance of tumors in peritoneal tumor mice injected with $Msln^{KD}$, ID8agg-luc cells treated with anti-PD-1 therapy were rechallenged intraperitoneally with ID8agg-luc cells. As a control, naïve female C57BL/6 mice were intraperitoneally injected with ID8agg-luc cells (n=6 per group). (M) Percentage of $CD69^-$ $CD103^-$, $CD69^+$ $CD103^-$, and $CD69^+$ $CD103^+$ cells among $CD44^+$ $CD8^+$ cells in ascites from mice, corresponding to (K). Data are shown as mean±SD. Statistical significance was assessed by two-way analysis of variance, followed by Tukey's post hoc test for multiple comparisons (B, D–J), log-rank test (C, L), and two-tailed unpaired Mann-Whitney U test (M). aPD1, anti-programmed cell death-1; Con, control; CXCL9, C-X-C motif chemokine ligand 9; HGSOC, high-grade serous ovarian cancer; IFN-γ, interferon-γ; IgG, immunoglobulin G; IVIS, In Vivo Imaging System; KD, knockdown; *Msln*, mesothelin; NS, no significant difference; PD-1, programmed cell death-1; Siglec-G, sialic acid-binding immunoglobulin-like lectin G; Siglec-10, sialic acid-binding immunoglobulin-like lectin 10; TCF-1, transcription factor T-cell factor-1; TNF-α, tumor necrosis factor-α.

ICB therapy and improving personalized treatment strategies. Ultimately, targeting MSLN could offer a promising strategy to enhance the responsiveness of patients with HGSOC to ICB therapy.

Previous studies have established that MSLN facilitates tumor cell proliferation, invasion, and migration through the aberrant activation of several signaling pathways.[10–12] Consistent with previous findings, we used proliferation assays to demonstrate that knockdown *Msln* significantly impaired tumor cell proliferation in murine ovarian cancer cell lines (online supplemental figure 8A–D), and this effect was more pronounced in OV2944-HM1 cells. Previous studies have suggested that MSLN is involved in reshaping the highly fibrotic TME in pancreatic ductal adenocarcinoma, thereby affecting immune cell infiltration and drug metabolism.[29] Based on these observations, we hypothesized that MSLN influences TME remodeling. However, the cellular and molecular mechanisms by which MSLN induces an immunosuppressive TME remain unclear. Unlike previous studies on colorectal cancer, which found that MSLN expression affected the infiltration of various immune cells, including macrophages, neutrophils, B cells, $CD4^+$, and $CD8^+$T cells,[30] our findings demonstrated a high degree of similarity in immunosuppressive patterns between patients with HGSOC and ovarian mouse models. Specifically, we observed an accumulation of protumorigenic TAMs and depletion of $CD8^+$ T cells in both MSLN-high HGSOC tissues and ascites from control tumor cell-bearing mice. *Msln* knockdown reversed this immunosuppressive TME and significantly extended the survival of tumor-bearing mice. Multiple potential mechanisms within malignant cells may lead to the polarization of macrophages towards a protumorigenic phenotype. For the first time, we identified and validated a direct ligand-receptor interaction between CD24 in $MSLN^+$ cancer cells and Siglec-10 in TAMs through in vivo and in vitro experiments. This interaction drives TAMs polarization towards a protumorigenic subtype, suppressing $CD8^+$ T-cell proliferation and activation. MSLN-targeting therapies have been reported to promote intratumoral $CD8^+$ T-cell infiltration.[7] Our study elucidated the detailed cellular and molecular mechanisms underlying this phenomenon.

This study is the first to propose that MSLN elevates CD24 expression by activating the Wnt/β-catenin signaling pathway. The Wnt/β-catenin pathway regulates the oncogenic processes of various solid tumors, including the promotion of cell proliferation, epithelial-mesenchymal transition, and maintenance of cancer stem cell self-renewal.[31–36] In breast and colorectal cancers, studies have reported that mutations in key components of the Wnt/β-catenin pathway, dysregulation of Wnt ligands and receptors, and epigenetic modifications contribute to tumorigenesis.[36–38] However, the role of the Wnt pathway in modulating TME in HGSOC remains unclear. Our study addresses this gap by providing preliminary insights into the cellular and molecular mechanisms by which the Wnt pathway influences TME alterations by promoting the expression of CD24 in HGSOC.

ICB therapy has revolutionized the treatment landscape for solid tumors; however, it has shown limited efficacy for ovarian cancer.[39] Targeting MSLN is considered an effective strategy to enhance antitumor immune responses and sensitize tumors to ICB treatment. The administration of LMB-100 to patients with mesothelioma has been observed to substantially enhance the effectiveness of anti-PD-1 therapy. This therapeutic approach has demonstrated an increase in treatment efficacy from below 20% to 40%, consequently impeding tumor progression.[7] In this study, we demonstrated that targeting MSLN could shift the immunosuppressive, non-responsive microenvironment to an immunoreactive, responsive one. *Msln* knockdown, in combination with anti-PD-1 treatment, significantly prolonged the survival of mice bearing intraperitoneal ID8agg tumors and induced the formation of tumor-specific immune memory. Based on these findings,

we propose that targeting MSLN is a promising strategy to enhance the effectiveness of ICB therapy against HGSOC.

Our study had several notable limitations. First, although we observed significant tumor growth inhibition with the combination of *Msln* knockdown in a cancer cell line and anti-PD-1 treatment in tumor-bearing mice, further investigation is required to determine whether LMB-100 combined with anti-PD-1 can achieve comparable results given that the antigen pool formed by MPF (Megakaryocyte Potentiating Factor) in the serum may result in antigen sink and off-target effects. Second, HGSOC exhibits site-specific TMEs, and immune cell composition varies across different anatomical sites in individual patients. In this study, we did not fully explore the differential impact of MSLN on the TME of primary and metastatic tumors. Large-scale clinical studies are required to validate the role of MSLN in enhancing ICB therapy efficacy.

In summary, the integration of computational analysis, animal studies, omics data, and functional data highlighted the role of MSLN as a key mediator of immune evasion. This study not only links MSLN to poor prognosis and immunosuppressive TME in HGSOC, but also provides evidence supporting MSLN as a promising target to enhance ICB efficacy, offering actionable insights for clinical decision-making.

Acknowledgements We would like to thank Dr X Tao and Dr J Zhao (Department of Pathology, Obstetrics and Gynecology Hospital of Fudan University, Shanghai, China) for their excellent pathological technology.

Contributors Haiou Liu and Jiaqi Lu conceived and designed the study. Yujing Zhong and Yiying Wang performed data acquisition, analysis, and interpretation of data. Kankan Cao, Xueling Wang, Chenyang Wang, Xuyao Xu, Moran Yang and Guodong Zhang provided the technical support. Haiou Liu, Jiaqi Lu and Yujing Zhong wrote the manuscript and all authors read and approved the final manuscript. YZ and YW contributed equally to this work. The corresponding author HL is the guarantor.

Funding This study was funded by National Science Foundation of China grants 82473274, 82273205, and 820721881 (to H. Liu) and 82203665 (to G. Zhang); Shanghai Clinical Research Center for Gynecological Diseases 22MC1940200 (to H. Liu); Natural Science Foundation of Shanghai grant 23ZR1408300 (to J. Lu); Shanghai Science and Technology Innovation Action Plan grant 23Y11909500 (to J. Lu) and 23Y11901800 (to G. Zhang). All study sponsors have no role in the study design, collection, analysis, and interpretation of data.

Competing interests No, there are no competing interests.

Patient consent for publication Not applicable.

Ethics approval This study involves human participants and was approved by the Ethics Committee of the Obstetrics and Gynecology Hospital, Fudan University (Kyy2016-49, Kyy2017-27, Kyy2022-158); the Ethics Committee of the Shanghai Cancer Center (050432-4-2108*). Participants gave informed consent to participate in the study before taking part.

Provenance and peer review Not commissioned; externally peer reviewed.

Data availability statement Data are available upon reasonable request.

ORCID iD

Haiou Liu http://orcid.org/0000-0003-0200-8981

REFERENCES

1 Konstantinopoulos PA, Waggoner S, Vidal GA, *et al*. Single-Arm Phases 1 and 2 Trial of Niraparib in Combination With Pembrolizumab in Patients With Recurrent Platinum-Resistant Ovarian Carcinoma. *JAMA Oncol* 2019;5:1141–1149.
2 Lv J, Li P. Mesothelin as a biomarker for targeted therapy. *Biomark Res* 2019;7:1–18.
3 Hassan R, Ho M. Mesothelin targeted cancer immunotherapy. *Eur J Cancer* 2008;44:46–53.
4 Pastan I, Hassan R. Discovery of mesothelin and exploiting it as a target for immunotherapy. *Cancer Res* 2014;74:2907–2912.
5 Chang K, Pastan I. Molecular cloning of mesothelin, a differentiation antigen present on mesothelium, mesotheliomas, and ovarian cancers. *Proc Natl Acad Sci U S A* 1996;93:136–140.
6 Cao B, Liu M, Wang L, *et al*. Use of chimeric antigen receptor NK-92 cells to target mesothelin in ovarian cancer. *Biochem Biophys Res Commun* 2020;524:96–102.
7 Jiang Q, Ghafoor A, Mian I, *et al*. Enhanced efficacy of mesothelin-targeted immunotoxin LMB-100 and anti-PD-1 antibody in patients with mesothelioma and mouse tumor models. *Sci Transl Med* 2020;12:1–12.
8 Liu W, Tai C-H, Liu X, *et al*. Anti-mesothelin immunotoxin induces mesothelioma eradication, anti-tumor immunity, and the development of tertiary lymphoid structures. *Proc Natl Acad Sci U S A* 2022;119:e2214928119.
9 Katz SI, Roshkovan L, Berger I, *et al*. Serum soluble mesothelin-related protein (SMRP) and fibulin-3 levels correlate with baseline malignant pleural mesothelioma (MPM) tumor volumes but are not useful as biomarkers of response in an immunotherapy trial. *Lung Cancer (Auckl)* 2021;154:5–12.
10 Servais EL, Colovos C, Rodriguez L, *et al*. Mesothelin overexpression promotes mesothelioma cell invasion and MMP-9 secretion in an orthotopic mouse model and in epithelioid pleural mesothelioma patients. *Clin Cancer Res* 2012;18:2478–2489.
11 Lurie E, Liu D, LaPlante EL, *et al*. Histoepigenetic analysis of the mesothelin network within pancreatic ductal adenocarcinoma cells reveals regulation of retinoic acid receptor gamma and AKT by mesothelin. *Oncogenesis* 2020;9:50–62.
12 Bharadwaj U, Marin-Muller C, Li M, *et al*. Mesothelin confers pancreatic cancer cell resistance to TNF-α-induced apoptosis through Akt/PI3K/NF-κB activation and IL-6/Mcl-1 overexpression. *Mol Cancer* 2011;10:92–106.
13 Hollevoet K, Mason-Osann E, Liu XF, *et al*. In vitro and in vivo activity of the low-immunogenic anti-mesothelin immunotoxin RG7787 in pancreatic cancer. 2019;13:2040–2049.
14 Kachala SS, Bograd AJ, Villena-Vargas J, *et al*. Mesothelin overexpression is a marker of tumor aggressiveness and is associated with reduced recurrence-free and overall survival in early-stage lung adenocarcinoma. *Clin Cancer Res* 2014;20:1020–1028.
15 Ravi A, Hellmann MD, Arniella MB, *et al*. Genomic and transcriptomic analysis of checkpoint blockade response in advanced non-small cell lung cancer. *Nat Genet* 2023;55:807–819.
16 Zhao H, Ming T, Tang S, *et al*. Wnt signaling in colorectal cancer: pathogenic role and therapeutic target. *Mol Cancer* 2022;21:110–144.
17 Yamamoto D, Oshima H, Wang D, *et al*. Characterization of RNF43 frameshift mutations that drive Wnt ligand- and R-spondin-dependent colon cancer. *J Pathol* 2022;257:39–52.
18 Parsons MJ, Tammela T, Dow LE. WNT as a Driver and Dependency in Cancer. *Cancer Discov* 2021;11:2413–2429.
19 Jiang P, Gu S, Pan D, *et al*. Signatures of T cell dysfunction and exclusion predict cancer immunotherapy response. *Nat Med* 2018;24:1550–1558.
20 Matulonis UA, Shapira-Frommer R, Santin AD, *et al*. Antitumor activity and safety of pembrolizumab in patients with advanced recurrent ovarian cancer: results from the phase II KEYNOTE-100 study. *Ann Oncol* 2019;30:1080–1087.

21 Keilholz U, Mehnert JM, Bauer S, *et al*. Avelumab in patients with previously treated metastatic melanoma: phase 1b results from the JAVELIN Solid Tumor trial. *J Immunother Cancer* 2019;7:1–12.
22 Clark CA, Gupta HB, Sareddy G, *et al*. Tumor-Intrinsic PD-L1 Signals Regulate Cell Growth, Pathogenesis, and Autophagy in Ovarian Cancer and Melanoma. *Cancer Res* 2016;76:6964–6974.
23 Drerup JM, Deng Y, Pandeswara SL, *et al*. CD122-Selective IL2 Complexes Reduce Immunosuppression, Promote Treg Fragility, and Sensitize Tumor Response to PD-L1 Blockade. *Cancer Res* 2020;80:5063–5075.
24 Barkal AA, Brewer RE, Markovic M, *et al*. CD24 signalling through macrophage Siglec-10 is a target for cancer immunotherapy. *Nature New Biol* 2019;572:392–396.
25 Pai SG, Carneiro BA, Mota JM, *et al*. Wnt/beta-catenin pathway: modulating anticancer immune response. *J Hematol Oncol* 2017;10:89–101.
26 Liu Z, Zhang Y, Ma N, *et al*. Progenitor-like exhausted SPRY1^{+}CD8^{+} T cells potentiate responsiveness to neoadjuvant PD-1 blockade in esophageal squamous cell carcinoma. *Cancer Cell* 2023;41:1852–1870.
27 Chen Z, Ji Z, Ngiow SF, *et al*. TCF-1-Centered Transcriptional Network Drives an Effector versus Exhausted CD8 T Cell-Fate Decision. *Immunity* 2019;51:840–855.
28 Virassamy B, Caramia F, Savas P, *et al*. Intratumoral CD8^{+} T cells with a tissue-resident memory phenotype mediate local immunity and immune checkpoint responses in breast cancer. *Cancer Cell* 2023;41:585–601.
29 Huang H, Wang Z, Zhang Y, *et al*. Mesothelial cell-derived antigen-presenting cancer-associated fibroblasts induce expansion of regulatory T cells in pancreatic cancer. *Cancer Cell* 2022;40:656–673.
30 Malla M, Deshmukh SK, Wu S, *et al*. Mesothelin expression correlates with elevated inhibitory immune activity in patients with colorectal cancer. *Cancer Gene Ther* 2024;31:1547–1558.
31 Liu J, Xiao Q, Xiao J, *et al*. Wnt/β-catenin signalling: function, biological mechanisms, and therapeutic opportunities. *Sig Transduct Target Ther* 2022;7:3–23.
32 Choi B-R, Cave C, Na CH, *et al*. GDE2-Dependent Activation of Canonical Wnt Signaling in Neurons Regulates Oligodendrocyte Maturation. *Cell Rep* 2020;31:1–24.
33 Wang Y, Krivtsov AV, Sinha AU, *et al*. The Wnt/beta-catenin pathway is required for the development of leukemia stem cells in AML. *Science* 2010;327:1650–1663.
34 Hawkins AG, Pedersen EA, Treichel S, *et al*. Wnt/β-catenin-activated Ewing sarcoma cells promote the angiogenic switch. *JCI Insight* 2020;5:e135188.
35 Unno K, Chalmers ZR, Pamarthy S, *et al*. Activated ALK Cooperates with N-Myc via Wnt/β-Catenin Signaling to Induce Neuroendocrine Prostate Cancer. *Cancer Res* 2021;81:2157–2170.
36 Zhou Y, Xu J, Luo H, *et al*. Wnt signaling pathway in cancer immunotherapy. *Cancer Lett* 2022;525:84–96.
37 Goss KH, Groden J. Biology of the adenomatous polyposis coli tumor suppressor. *J Clin Oncol* 2000;18:1967–1979.
38 Zhang L, Shay JW. Multiple Roles of APC and its Therapeutic Implications in Colorectal Cancer. *J Natl Cancer Inst* 2017;109:djw332.
39 Disis ML, Taylor MH, Kelly K, *et al*. Efficacy and Safety of Avelumab for Patients With Recurrent or Refractory Ovarian Cancer: Phase 1b Results From the JAVELIN Solid Tumor Trial. *JAMA Oncol* 2019;5:393–401.